Point to point response to reviewer RC2

Citation of the review: https://doi.org/10.5194/egusphere-2022-673-RC2

We thank the reviewer for the valuable feedback and constructive comments. Below you will find the detailed responses to all the reviewer's comments. The reviewer's comments are highlighted in red, our comments are in black.

The paper analyses the process of infiltration of a liquid into an unsaturated porous medium, which is characterized by different regimes depending on the level of saturation. The liquid is assumed to be wettable with respect to the homogeneous medium. Then, the authors introduce a semi-continuum model that lends itself well to the interpretation of the infiltration regime.

The topic is of interest and deals with a process that even in extremely simple situations reveals a degree of complexity.

Major issue 1: However, I see the major limitation in the absence of experimental validation: the numerical scheme, although of interest, appears limited in its interpretation of physical reality.

We agree that a more detailed explanation of the semi-continuum model should be included in the manuscript to make the manuscript easier to understand. Since reviewer RC1 raised a similar comment, we copied the response to the reviewer RC1 below.

The concept of the semi-continuum model is closely related with the scaling of the retention curve (see Figure 1 in the manuscript). Understanding this concept may not be clear, so we provide a brief discussion below that we plan to include in the manuscript. However, the detailed mathematical and physical justification is already published in [1], hence for a deeper understanding we refer to this paper.

The scaling of the retention curve, i.e. the dependence of the capillary pressure-saturation relation on the block size, is not a common approach in flow modelling. However, the dependence of the experimentally determined retention curve on the porous medium sample size has been observed for a long time [2, 3, 4, 5, 6, 7]. The concept of REV is essential in this case because if the sample of porous medium is smaller than REV, key physical quantities, such as the retention curve, are strongly dependent on the sample size. The crucial idea of the semi-continuum model is to include this dependency in the model, i.e. to scale the retention curve according to the block size. In the semi-continuum model, a block represents a real sample of the porous material. This makes the semi-continuum model fundamentally different from numerical schemes for solving partial differential equations where the block plays only a discretization (i.e. mathematical) role and regardless of the block size, the retention curve remains the same. In the semi-continuum model, the computational mesh (the blocks) takes into account the dependence of the physical parameters on the size of the blocks. Surprisingly, the idea of taking REV size into account in modelling porous media has been around for a long time. For instance, in [8], the authors estimated the size of the REV and used it as a lower limit for the size of the finite elements. They argue that the use of smaller elements would lead to violation of continuum assumptions and thus the continuum approximation would no longer be appropriate. The same idea is used in the semi-continuum model: For blocks smaller than the REV, scaling of the retention curve must be included because the continuum approximation is no longer adequate. Because we are interested in the description of flow phenomena below the REV scale, we need to include the dependence of the retention curve on the block size. This scaling of the retention curve must meet a physically justified requirement that the nature of the flow is preserved across all levels of block size. This means that the fluxes between neighboring blocks must not change when Δx changes. Given equation (4) in the manuscript, if Δx decreases by half, the fluxes increase by a factor of two if the scaling of the retention curve is not included. Therefore, a linear scaling of the retention curve is introduced in equation (6) in the manuscript, so the fluxes between blocks remain the same as Δx decreases. For more details, see figures Fig. 4–6 in [1] that show the numerical convergence of the semi-continuum model in 1D and 2D.

The natural question is what the limit of the semi-continuum model would be as $\Delta x \to 0$. We tried to answer this question in [1] and derived the limit equation in a single spatial dimension:

$$(K_{PS}\partial_t S - \partial_t P_H)\,(P_H - v) \geq 0, \qquad \text{for all } v \in [C_2, C_1], \qquad \text{and } P_H \in [C_2, C_1],$$

$$\theta\partial_t S + \partial_x\left(\frac{\kappa}{\mu}\sqrt{k(S^-)}\sqrt{k(S^+)}(\rho g - \partial_x P_H)\right) = 0, \qquad S^{\pm}(x_0,t) = \lim_{x\to x_0^{\pm}} S(x,t).$$

In this equation, κ denotes the intrinsic permeability, ρ the fluid density, g acceleration due to gravity, μ the dynamic viscosity of fluid, and S the saturation. The values C_1 [Pa] and C_2 [Pa] denote the constant limits of the main wetting and draining branches, respectively. The limit is a partial differential equation containing a Prandtl-type hysteresis operator P_H under the space derivative. If we are located on the main wetting or draining branches, the limit equation becomes a hyperbolic differential equation. Between the two main branches (i.e., we are located on the scanning curve), the limit represents a parabolic differential equation. It means the limit switches between parabolic and hyperbolic types of equation. The limit equation is a new type of mathematical model – we are not aware of any research that has investigated equations of this type. Note that the Richards' equation is a parabolic type equation – that is why it is only able to simulate the diffusion-like flow regime [9].

Major issue 2: Moreover, and this is a second major issue, there is a lack of sensitivity analysis, since the only estimator comes from repeating the numerical tests by changing only the intrinsic permeability distribution. In this sense, it is necessary for the authors to thoroughly analyse the uncertainty of the parameters (viscosity, degree of saturation, etc.) and analyse the variability of the governed quantities.

We agree and provide the sensitivity analysis. All the simulations are computationally demanding, and so distributed computing infrastructure "e-Infrastruktura CZ" (e-INFRA LM2018140) has been used. The sensitivity analysis was performed by varying intrinsic permeability, dynamic viscosity, relative permeability, retention curve and the boundary flux. This was done for four different distributions of the intrinsic permeability and seven different values of initial saturation. In total, 588 simulations were performed. However, for the block size that is used in the manuscript ($\Delta x = 0.25$ cm), a single simulation takes almost 30 days. Thus, the sensitivity analysis could not be performed for $\Delta x = 0.25$ cm. Therefore, a larger block size $\Delta x = 0.50$ cm was used while the rest of parameters remained the same as in the manuscript. Let us note that even with the larger block size, all the simulations took almost 1000 CPU days.

The results of the sensitivity analysis are presented below. It is demonstrated that the Bauters' paradox occurs for different values of material parameters or different boundary conditions. Some figures related to the sensitivity analysis are included at the end of this response so that this text is not too extensive. We suggest to include these figures in the appendix of the manuscript.

Effect of the intrinsic permeability and dynamic viscosity on the flow regime

Increasing the intrinsic permeability κ has the same effect as decreasing the parameter μ and vice versa. Therefore, a fraction $\frac{\kappa}{\mu}$ is used for the sensitivity analysis of both these parameters. The baseline values of κ and μ are given in Table 1 in the manuscript. Five different values $b \cdot \frac{\kappa}{\mu}$ were examined, where $b = 0.50$, 0.75, 1.00, 1.50 and 2.00. Obviously, baseline simulations are given for $b = 1.00$. For each value of b, 28 different simulations are performed, with variable initial saturation (seven different initial saturation) and variable intrinsic permeability distribution (four different distributions). To generate spatially correlated distribution of the intrinsic permeability, the same approach was used as in the manuscript; see Fig. A.1 at the end of this response. Note that 140 different simulations were performed in total. The same scheme was applied to all other sensitivity analysis simulations, i.e. the analysis was always performed for seven different values of initial saturation and four different distributions of intrinsic permeability.

Figure 1 shows the width and the velocity of the fingers (moisture profiles) 25 minutes from the beginning of infiltration for five different values of b and for seven different values of initial saturation S_{in}. The width of each moisture profile was calculated in the same way as in the manuscript. For a given value b and S_{in}, the average width and velocity of the moisture profile of four different distributions of the intrinsic permeability were calculated and plotted.

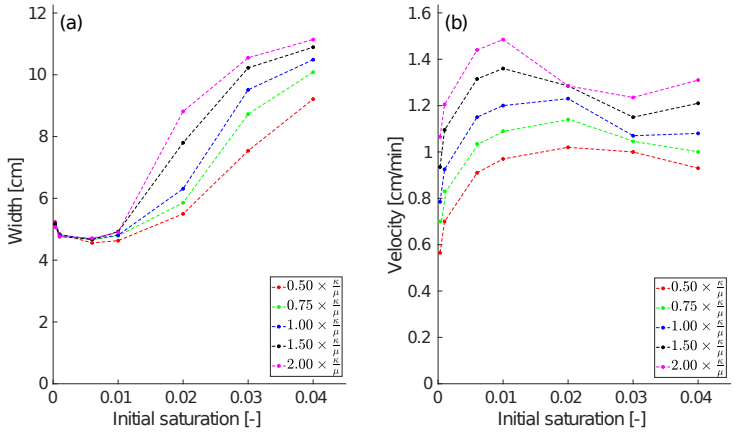

Figure 1: The effect of the intrinsic permeability and dynamic viscosity on the flow regime. The width **(a)** and the velocity **(b)** of the finger (or wetting front) at $t = 25$ minutes is plotted against the initial saturation for five different values of $b \cdot \frac{\kappa}{\mu}$. The average of four different distributions of the intrinsic permeability is plotted.

It can be seen in Fig. 1**(a)** that as parameter b increases, the width of the moisture profiles increases for higher initial saturation. For lower initial saturation, the effect of b is negligible. This is because with increasing parameter b, diffusion-like behavior is observed for lower values of initial saturation. The transition between the finger-like and diffusion-like regimes is clearly evident for the initial saturation, for which the width of the moisture profiles increases rapidly. For instance, for $b = 2.00$ and $b = 1.50$, the rapid increase can be already seen for $S_{in} = 0.02$. For lower values of b, diffusion-like behavior is observed for higher values of initial saturation. To make this as clear as possible, a snapshot of the saturation field at 25 minutes for the intrinsic permeability distribution defined by Fig. A.1**(a)** is shown in Fig. A.2 at the end of this response. As for the moisture profile width, the velocity of the moisture profiles also increases with increasing b as can be seen in Fig. 1**(b)**. This is expected because the parameter b affects directly the magnitude of the flow.

Finally, it can be seen that the Bauters' paradox is observed for all values of b. Therefore, the non-monotonic behavior of the width and the velocity of the moisture profiles is not dependent on intrinsic permeability and/or dynamic viscosity.

Effect of relative permeability on the flow regime

The relative permeability function $k(S)$ is given by equation (3) in the manuscript. The function contains a free parameter $\lambda[-]$ and therefore the effect of the relative permeability on the flow regime is tested by using five different values of λ ranging from 0.6 to 1.0. The baseline simulations are given for $\lambda = 0.8$. Note that the parameter λ affects the value of the relative permeability especially for an initially dry porous medium. For the lowest initial saturation used for simulations ($S_{in} = 0.0003$), the relative permeability is more than 25 times larger for $\lambda = 0.6$ compared to $\lambda = 1.0$. In contrast, it is approximately 3.6 times larger for $S_{in} = 0.04$. As mentioned above, 28 different simulations were performed for each λ with variable initial saturation and intrinsic permeability distribution. Again, a snapshot of the saturation field at 25 minutes for the intrinsic permeability distribution defined by Fig. A.1**(a)** is shown in Fig. A.3 at the end of this response..

Figure 2 shows the width and the velocity of the fingers (moisture profiles) 25 minutes from the beginning of infiltration for five different values of λ and for seven different values of initial saturation S_{in}. For a given value of λ and S_{in}, the average width and velocity of the four different distributions of the intrinsic permeability is calculated and plotted. With decreasing λ (the relative permeability is increasing), the diffusion-like behavior is observed for lower initial saturation, hence the width of the moisture profile is increasing. This is expected because the effect of relative permeability on the flow regime should be similar to the effect of intrinsic permeability and dynamic viscosity, see Fig. 1**(a)**. Note that the effect of relative permeability is more pronounced because the relative permeability varies more significantly for different values of λ compared to the sensitivity analysis shown in Fig. 1.

The velocity of the moisture profiles is increasing with decreasing λ for lower initial saturation values. However, this does not apply for initial saturation $S_{in} = 0.02$ and higher. This is because for lower λ, a diffusion-like behavior is observed for lower values of initial saturation, hence the moisture profile slows down significantly.

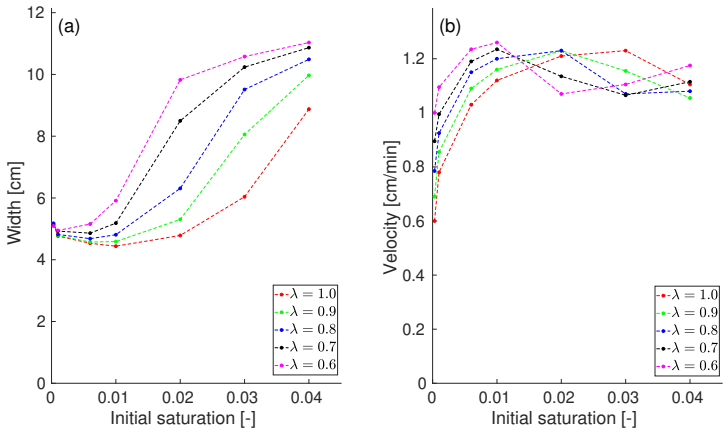

Figure 2: The effect of the relative permeability on the flow regime. The width **(a)** and the velocity **(b)** of the finger (or wetting front) at $t = 25$ minutes is plotted against the initial saturation for five different values of parameter λ. The average of four different distributions of the intrinsic permeability is plotted.

The Bauters' paradox is again observed for all values of λ. As λ increases, both the minimum width and maximum velocity occur for higher values of initial saturation. This is because the diffusion-like behavior occurs at higher values of initial saturation. The manifestation of the Bauters' paradox is thus shifted to higher initial saturation values. This can also be seen in Fig. 1, but the effect is not so pronounced.

Effect of the retention curve on the flow regime

The effect of the retention curve on the flow regime is tested using different parameters α_w and α_d related to the main wetting and main draining branches, respectively. This is done by multiplying the basic values of the parameters α_w and α_d (given in Table 1 in the manuscript) by the free parameter α. Both values α_w and α_d are multiplied by the same parameter α ranging from 0.70 to 1.30. Obviously, the baseline simulations are given for $\alpha = 1.00$. The parameters n_w and n_d are fixed and are given in Table 1 in the manuscript.

Note that with increasing α, the main branches become flatter. This is analogous to using a porous medium with coarser grains. On the other hand, as α decreases, the main branches get steeper, analogous to using a porous medium with finer grains. Figure 3 shows the width and the velocity of the fingers (moisture profiles) 25 minutes from the beginning of infiltration for five different values of α and for seven different values of initial saturation S_{in}. For a given value α and S_{in}, the average width and velocity of the four different distributions of the intrinsic permeability is calculated and plotted. Again, a snapshot of the saturation field at 25 minutes for the intrinsic permeability distribution defined by Fig. A.1**(a)** is shown in Fig. A.4 at the end of this response. As α decreases, the width of the moisture profiles increases rapidly because the diffusion-like behavior is observed for lower values of initial saturation. This is consistent with experimental observations, as the diffusion-like behavior is more readily observed in porous media with finer grains compared to coarser grains; see e.g. the experiments in Cremer et al. [10]. Next, the velocity of the moisture profiles decreases as α decreases. This is expected because at lower values of α, the flow behaves much more diffusion-like and therefore the moisture profiles are slower. See Fig. A.4 at the end of this response for more details.

The Bauters' paradox occurs for all tested values α. Moreover, similarly to the effect of the relative permeability, the minimum width and maximum velocity occur for higher initial saturation as α increases, so that the manifestation of the Bauters' paradox is shifted to higher initial saturation values.

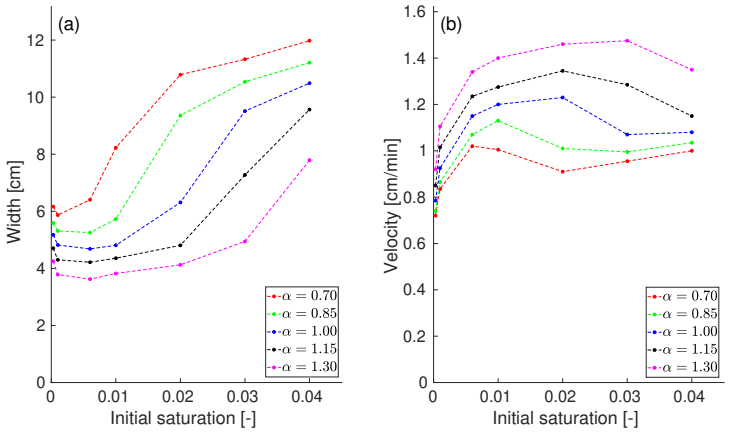

Figure 3: The effect of the retention curve on the flow regime. The width **(a)** and the velocity **(b)** of the finger (or wetting front) at $t = 25$ minutes is plotted against the initial saturation for five different values of parameter α. The averages of four different distributions of the intrinsic permeability are plotted.

Effect of the boundary flux on the flow regime

Finally, sensitivity analysis for the boundary flux q_B is performed. Five different values of the boundary flux were used ranging from 2×10^{-5} ms^{-1} to 16×10^{-5} ms^{-1}. The baseline simulations are given for $q_B = 8 \times 10^{-5}$ ms^{-1}. Figure 4 shows the width and the velocity of the fingers (moisture profiles) for five different values of boundary flux q_B and for seven different values of the initial saturation S_{in}. For a given value q_B and S_{in}, the average width and velocity of the four different distributions of the intrinsic permeability is calculated and plotted. Snapshot of the saturation field for the intrinsic permeability distribution defined by Fig. A.1**(a)** is shown in Fig. A.5 at the end of this response. Since the used boundary fluxes varied by more than one order of magnitude, the times for which the velocity and the width are calculated need to be scaled according to the boundary flux. The time-points used were $t = 100, 50, 25, 12.5$ and 6.25 minutes for $q_B = 2, 4, 8, 16, 32 \times 10^{-5}$ ms^{-1}, respectively. It can be seen in Fig. 4**(a)** that with decreasing boundary flux, the flow tends to become more diffusive. This is in good agreement with the experimental observation [11]. Moreover, it is not surprising that the velocity of the moisture profiles shown in Fig. 4**(b)** decreases with decreasing boundary flux.

The Bauters' paradox is again observed for all tested values of q_B, so that the manifestation of the Bauters' paradox shifts towards higher initial saturation values as the boundary flux increases.

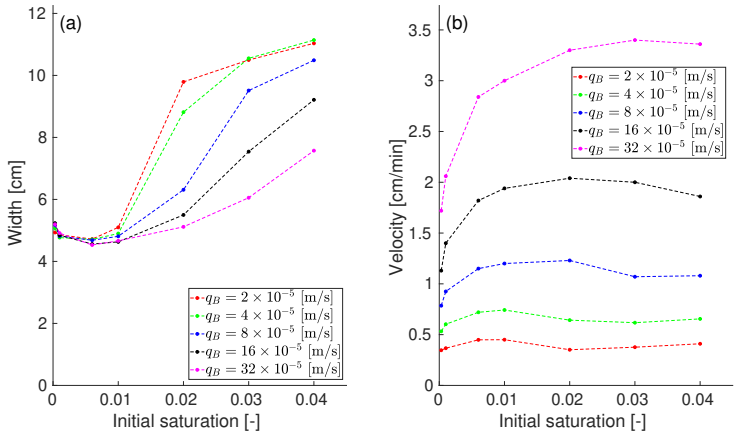

Figure 4: The effect of the boundary flux on the flow regime. The width **(a)** and the velocity **(b)** of the finger (or wetting front) is plotted against the initial saturation for five different values of boundary flux q_B. Times are scaled according to the boundary flux q_B, thus the width and velocity of the moisture profiles are calculated at $t = 100, 50, 25, 12.5$ and 6.25 minutes for $q_B = 2, 4, 8, 16, 32 \times 10^{-5}$ ms^{-1}, respectively. The averages of four different distributions of the intrinsic permeability are plotted.

Major issue 3: There is one point of particular interest: if Bauter's paradox occurs even when intrinsic permeability is homogeneous, how does the proposed model behave in this situation?

As stated in the text of the manuscript (lines 214–216), the Bauters' paradox with constant intrinsic permeability can be observed in Fig. 4.3 in the Dissertation Thesis [12]. However, more physical-looking fingers evolve if the distribution of the intrinsic permeability is included. We believe that including the simulations in the Appendix of the manuscript for the case of homogeneous intrinsic permeability is more appropriate than referring to the Dissertation. Therefore, the same simulations as in the manuscript have been performed with homogeneous intrinsic permeability. The parameters used for simulations are given in Table 1 in the manuscript. Figure 5 shows a snapshot of the saturation field at 25 minutes for seven different values of the initial saturation. It is observed that the Bauters' paradox occurs even in this case. The effect of the intrinsic permeability distribution is pronounced for the initially dry porous medium, while for the initially wet porous medium this effect is negligible. This is expected because in the case of diffusion-like regime, small changes in intrinsic permeability do not have a significant effect on the flow. The artificial looking behavior for the initially dry porous medium is eliminated if a more realistic porous medium is used for the simulations, i.e. if the distribution of the intrinsic permeability is included.

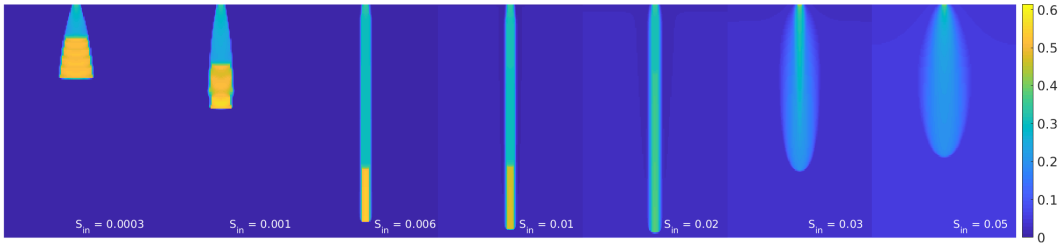

Figure 5: Snapshot of the saturation field at 25 minutes for seven different values of the initial saturation. The distribution of the intrinsic permeability is not included, i.e. the medium is perfectly homogeneous. Saturation values are colour-coded according to the colour bar on the right. Initial saturation of the medium increases from left to right.

Major issue 4: Last, the authors tell us about the behavior of their model, but the interpretation of why appears to be missing.

We agree with the reviewer that interpretation/explanation why the Bauters' paradox occurs is missing. We suggest to include the following explanation in the manuscript.

We conjecture that the explanation of the Bauters' paradox is rather similar to the non-monotonic dependence of porous medium flow on the magnitude of the influx. For very small values of influx, the flow becomes stable with increasing finger width. The same applies for very large values of influx. Hence, the unstable flow is only observed for fluxes within a certain range [13, 14, 15]. Yao and Hendrickx [13] hypothesized that the stable flow occurs when the effect of gravity becomes negligible. This happens in two "extreme" cases. First, at very low infiltration rates, capillarity becomes the dominant force compared to the force of gravity. Second, for infiltration rates higher than the saturated hydraulic conductivity, the viscosity dominates and the stable flow without fingers occurs. In our case, the dependence of the flow regime on the initial saturation behaves similarly. For initially dry porous medium, the capillarity dominates and the large capillary forces are able to win over gravity in sucking the water sideways into dry areas of the matrix. In a medium, which is moderately wet, this becomes more difficult, because the capillary forces are generally lower. Thus, in a moderately wet medium, the fingers become thinner and faster. At sufficiently high initial saturation, the large conductivity between neighboring blocks prevents water piling up behind the wetting front and the formation of saturation overshoot. This results in the ability of lateral expansion because the persistence of the fingers is suppressed [16, 17]. Therefore, a diffusion-like flow regime is observed.

Minor comments:

1. Figure 3: specify units for the colorbar
2. Figures 5-6: add the frame to panel b diagram

These minor issues will be fixed in the manuscript.

References

[1] R. Vodák, T. Fürst, M. Šír, and J. Kmec, "The difference between semi-continuum model and richards' equation for unsaturated porous media flow," *Scient. Rep.*, vol. 12, p. 7650, 2022.

[2] R. G. Larson and N. R. Morrow, "Effects of sample size on capillary pressures in porous media," *Powder Technology*, vol. 30(2), pp. 123–138, 1981.

[3] B. K. Mishra and M. M. Sharma, "Measurement of pore size distributions from capillary pressure curves," *American Institute of Chemical Engineers Journals*, vol. 34(4), pp. 684–687, 1988.

[4] D. Zhou and E. H. Stenby, "Interpretation of capillary-pressure curves using invasion percolation theory," *Transport Porous Med.*, vol. 11, pp. 17–31, 1993.

[5] E. Perfect, L. D. McKay, S. C. Cropper, S. G. Driese, G. Kammerer, and J. H. Dane, "Capillary pressure–saturation relations for saprolite: Scaling with and without correction for column height," *Vadose Zone Journal*, vol. 3(2), pp. 493–501, 2004.

[6] A. G. Hunt, R. P. Ewing, and R. Horton, "What's wrong with soil physics," *Soil Science Society of America Journal*, vol. 77, p. 1877– 1887, 2013.

[7] B. Ghanbarian, V. Taslimitehrani, G. Dong, and Y. A. Pachepsky, "Sample dimensions effect on prediction of soil water retention curve and saturated hydraulic conductivity," *Journal of Hydrology*, vol. 528, pp. 127–137, 2015.

[8] J. A. White, R. I. Borja, and J. T. Fredrich, "Calculating the effective permeability of sandstone with multiscale lattice boltzmann/finite element simulations," *Acta Geotechnica*, vol. 1, pp. 195–209, 2006.

[9] T. Fürst, R. Vodák, M. Šír, and M. Bíl, "On the incompatibility of richards' equation and finger-like infiltration in unsaturated homogeneous porous media," *Water Resour. Res.*, vol. 45(3), p. W03408, 2009.

[10] C. J. M. Cremer, C. Schuetz, I. Neuweiler, P. Lehmann, and E. H. Lehmann, "Unstable infiltration experiments in dry porous media," *Vadose Zone J.*, vol. 16 (7), 2017.

[11] D. A. DiCarlo, "Experimental measurements of saturation overshoot on infiltration," *Water Resour. Res.*, vol. 40(4), p. W04215, 2004.

[12] J. Kmec, *Analysis of the mathematical models for unsaturated porous media flow, Ph.D. thesis.* Palacký University in Olomouc, Czech Republic, 2021.

[13] T. Yao and J. M. H. Hendrickx, "Stability of wetting fronts in dry homogeneous soils under low infiltration rates," *Soil Sci. Soc. Am. J.*, vol. 60, pp. 20–28, 1996.

[14] R. J. Glass, J.-Y. Parlange, and T. S. Steenhuis, "Wetting front instability. 2. experimental determination of relationships between system parameters and two-dimensional unstable flow field behavior in initially dry porous media," *Water Resour. Res.*, vol. 25(6), pp. 1195–1207, 1989.

[15] D. A. DiCarlo, "Stability of gravity-driven multiphase flow in porous media: 40 years of advancements," *Water Resour. Res.*, vol. 49, pp. 4531–4544, 2013.

[16] F. Rezanezhad, H.-J. Vogel, and K. Roth, "Experimental study of fingered flow through initially dry sand," *Hydrol. E. Sys. Sci. D.*, vol. 3(4), pp. 2595–2620, 2006.

[17] J. Kmec, T. Fürst, R. Vodák, and M. Šír, "A two dimensional semi-continuum model to explain wetting front instability in porous media," *Scient. Rep.*, vol. 11, p. 3223, 2021.

A Figures

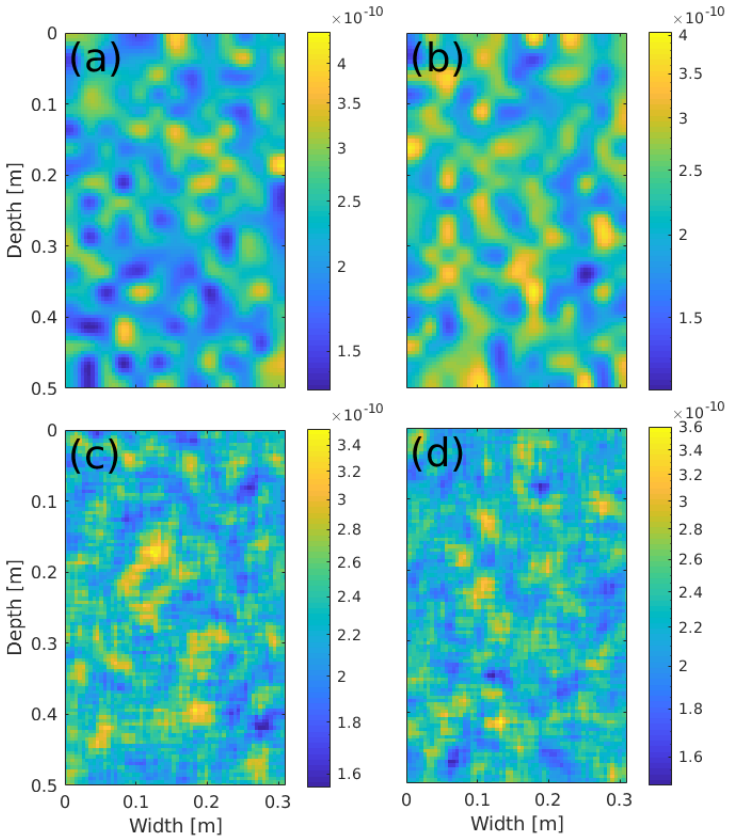

Figure A.1: The distribution of the intrinsic permeability. The distributions satisfy: **(a)** $\kappa_{max}/\kappa_{min} \approx 3.40$, **(b)** $\kappa_{max}/\kappa_{min} \approx 3.48$, **(c)** $\kappa_{max}/\kappa_{min} \approx 2.28$, **(d)** $\kappa_{max}/\kappa_{min} \approx 2.42$. Intrinsic permeability values are colour-coded according to the colour bar on the right.

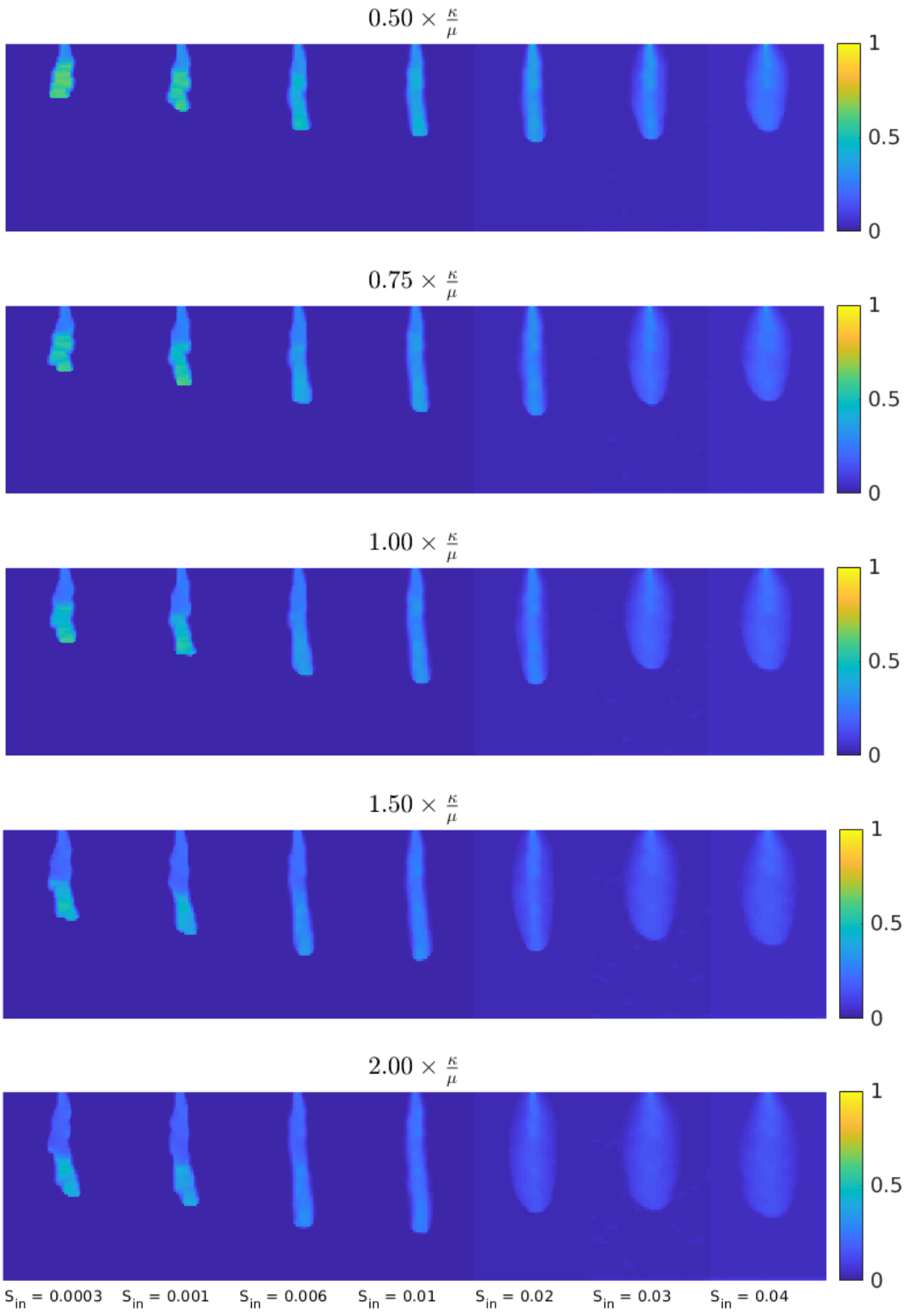

Figure A.2: A snapshot of the saturation field at 25 minutes for the intrinsic permeability distribution shown in Fig. A.1**(a)** for five different values of b and for seven different values of initial saturation S_{in}.

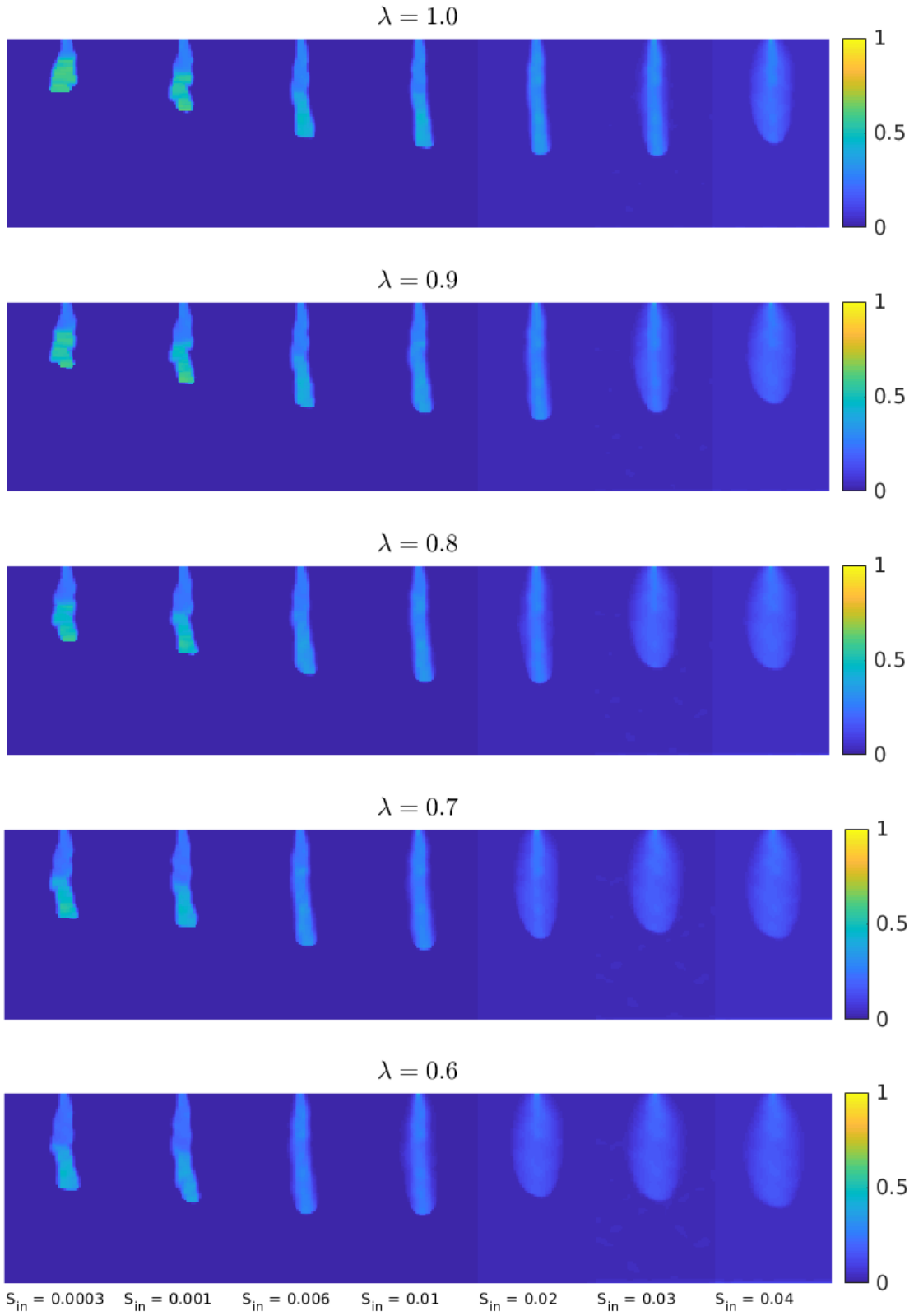

Figure A.3: A snapshot of the saturation field at 25 minutes for the intrinsic permeability distribution shown in Fig. A.1**(a)** for five different values of λ and for seven different values of initial saturation S_{in}.

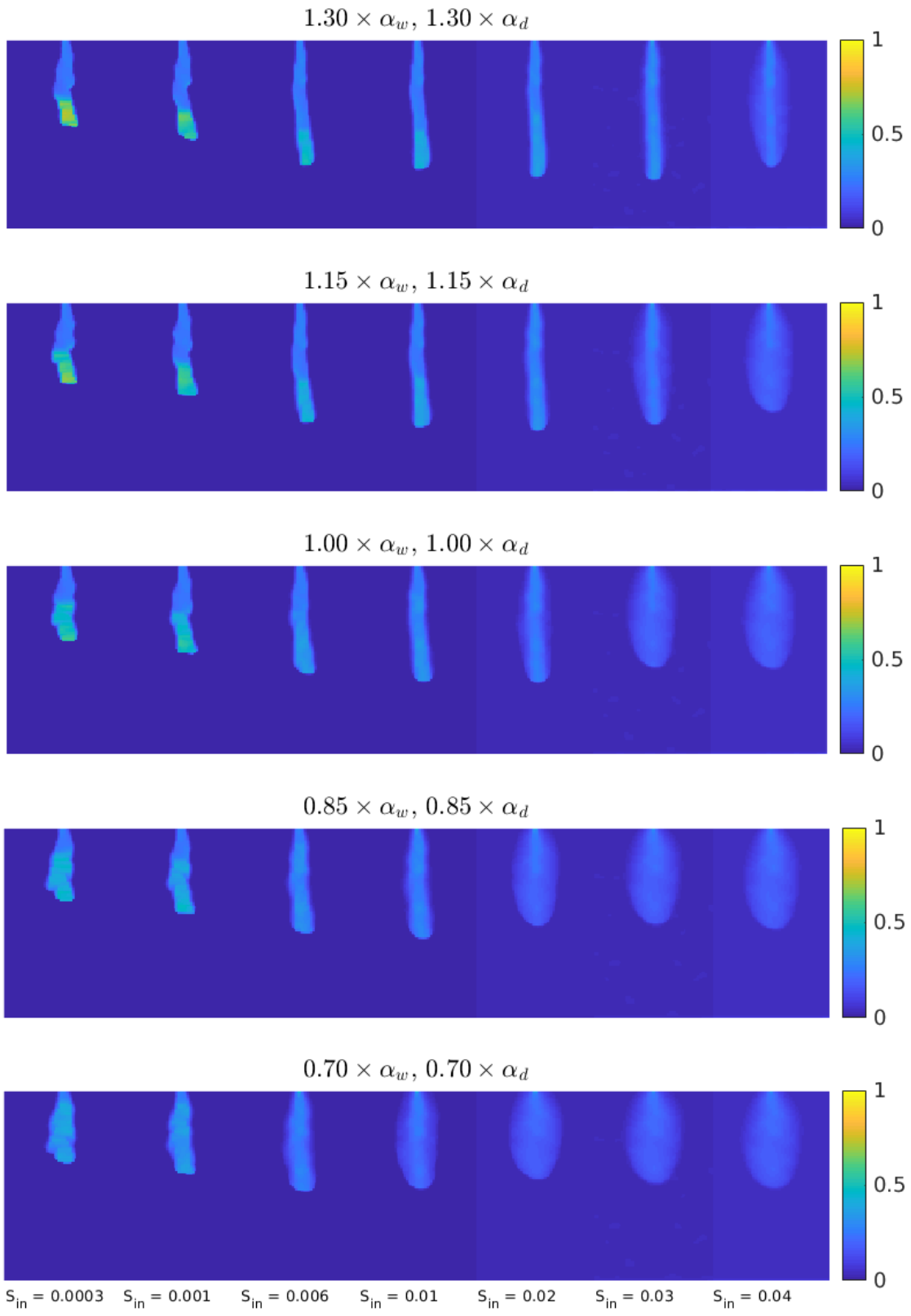

Figure A.4: A snapshot of the saturation field at 25 minutes for the intrinsic permeability distribution shown in Fig. A.1**(a)** for five different values of α and for seven different values of initial saturation S_{in}.

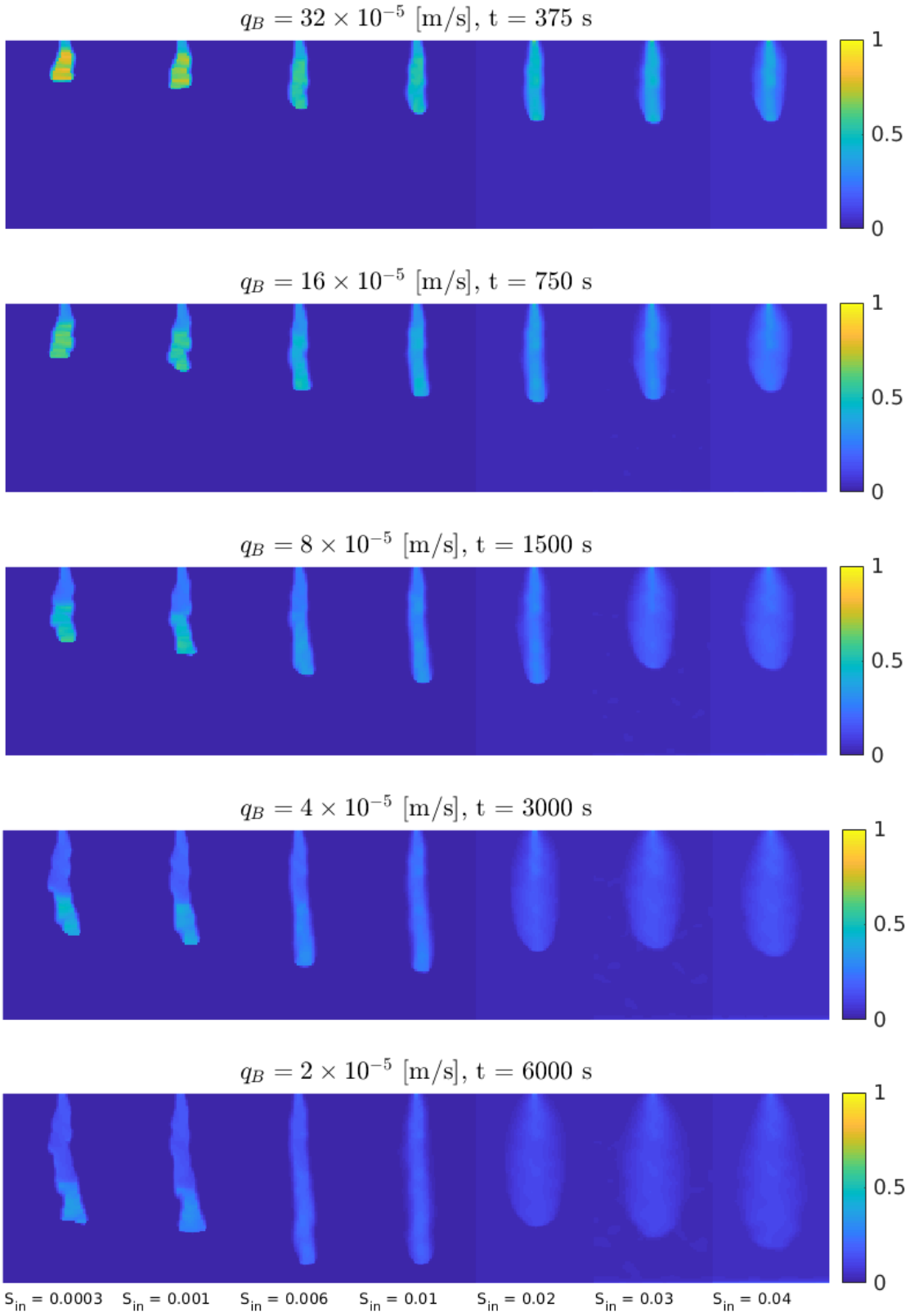

Figure A.5: A snapshot of the saturation field for the intrinsic permeability distribution shown in Fig. A.1**(a)** for five different values of q_B and for seven different values of initial saturation S_{in}. Times are scaled according to the boundary flux q_B, thus a snapshot of the saturation field is shown at $t = 100, 50, 25, 12.5$ and 6.25 minutes for $q_B = 2, 4, 8, 16, 32 \times 10^{-5}$ ms^{-1}, respectively.